

# Structural and functional evidence that Rad4 competes with Rad2 for binding to the Tfb1 subunit of TFIIH in NER

Julien Lafrance-Vanasse, Geneviève Arseneault, Laurent Cappadocia, Pascale Legault and James G. Omichinski\*

Département de Biochimie, Université de Montréal C.P. 6128 Succursale Centre-Ville, Montréal, Québec, Canada H3C 3J7

Received October 12, 2012; Revised November 19, 2012; Accepted November 20, 2012

## ABSTRACT

**XPC/Rad4 (human/yeast) recruits transcription factor IIH (TFIIH) to the nucleotide excision repair (NER) complex through interactions with its p62/Tfb1 and XPB/Ssl2 subunits. TFIIH then recruits XPG/Rad2 through interactions with similar subunits and the two repair factors appear to be mutually exclusive within the NER complex. Here, we show that Rad4 binds the PH domain of the Tfb1 (Tfb1PH) with high affinity. Structural characterization of a Rad4–Tfb1PH complex demonstrates that the Rad4-binding interface is formed using a motif similar to one used by Rad2 to bind Tfb1PH. *In vivo* studies in yeast demonstrate that the N-terminal Tfb1-binding motif and C-terminal TFIIH-binding motif of Rad4 are both crucial for survival following exposure to UV irradiation. Together, these results support the hypothesis that XPG/Rad2 displaces XPC/Rad4 from the repair complex in part through interactions with the Tfb1/p62 subunit of TFIIH. The Rad4–Tfb1PH structure also provides detailed information regarding, not only the interplay of TFIIH recruitment to the NER, but also links the role of TFIIH in NER and transcription.**

## INTRODUCTION

Exposure to ultraviolet (UV) irradiation can threaten the survival of organisms due to its ability to damage DNA by inducing modifications such as cyclobutane pyrimidine dimers (CPD) and (6,4) photoproducts (6,4PP). Due to the constant threat that UV irradiation poses, organisms

have developed pathways like nucleotide excision repair (NER) to repair the damaged DNA (1). Failure to repair the damage ultimately threatens the integrity of the organism's genome, and it is now clear that defects in factors that function in the NER repair pathway results in a number of debilitating human diseases including xeroderma pigmentosum (XP) (2). XP is an autosomal recessive genetic disorder characterized by a hypersensitivity to UV irradiation, and the most common human form of XP is associated with mutations of the complementation group XP-C (3). XP patients are defective in their ability to perform NER following exposure to UV irradiation, which results in an increased probability of acquiring a number of different forms of skin cancers (4).

NER can be divided into two pathways depending on whether the damaged DNA that needs to be repaired is being actively transcribed (transcription-coupled NER; TC-NER) or not (global genome NER; GG-NER). Although these two pathways of NER share many similarities, they differ considerably in how the damaged DNA is initially recognized. In GG-NER, the XPC-RAD23B/Rad4-Rad23 (human/yeast) complex recognizes the damaged DNA, sometimes with the help of UV-DDB (UV-damaged DNA-binding factor) (5,6). In contrast, during TC-NER, the RNA polymerase II (RNAP II) complex stalls on the damaged site, which leads to the recruitment of the Cockayne syndrome B (CSB/Rad26) protein (7,8). Following this initial recognition of the damaged DNA site, the second step of both NER pathways involves the recruitment of the general transcription factor IIH (TFIIH) due to the presence of either CSB/Rad26 (TC-NER) or XPC/Rad4 (GG-NER) (7–11).

As a crucial component of the GG-NER pathway, XPC/Rad4 participates in a number of protein–protein

\*To whom correspondence should be addressed. Tel: +1 514 343 7341; Fax: +1 514 343 2210; Email: jg.omichinski@umontreal.ca

and protein–DNA interactions. Studies with the full-length XPC/Rad4 demonstrated that the central region of Rad4 (residues 120–630) was sufficient for both specific binding to the CPD-damaged DNA and heterodimerization with Rad23 (12). These studies also concluded that the amino-terminal (N-terminal; residues 1–120) and carboxyl-terminal (C-terminal; residues 630–754) regions of Rad4 are most likely disordered based on their sensitivity to proteolysis and this is consistent with nuclear magnetic resonance (NMR) studies showing that the C-terminal 125 amino acids of XPC (residues 816–940) are also disordered (13). Despite being disordered, several studies have shown that the N- and C-terminal regions of XPC/Rad4 play important roles in interactions with Centrin-2, Cdc31, Rad33 and TFIIH (9,14–17).

TFIIH is a 10-subunit complex that is highly conserved between humans and budding yeast (*Saccharomyces cerevisiae*). Once recruited to the damaged DNA site by XPC/Rad4, TFIIH plays several important functions. First, through the helicase activities of its XPB/Ssl2 and XPD/Rad3 subunits, TFIIH assists in unwinding the DNA in and around the damaged site (18). Next, TFIIH recruits the 3'-endonuclease XPG/Rad2, which initiates the cutting of the DNA and the subsequent excision/repair processes (19). In GG-NER, the recruitment of XPG/Rad2 to the damaged DNA site coincides with the release of the XPC-RAD23B/Rad4–Rad23 complex, and this exchange between XPC/Rad4 and XPG/Rad2 appears to be mediated through interactions involving TFIIH (10,20,21). As a result, a number of studies have examined the interaction between TFIIH and XPC/Rad4 to understand its role in NER. Co-immunoprecipitation (Co-IP) studies with Rad4 indicated that residues 1–167 are sufficient for binding to TFIIH (9). In addition, *in vitro* and *in vivo* studies showed that both the XPB and p62 subunits of TFIIH directly interact with XPC and that the C-terminal region of XPC plays an important role in recruiting the TFIIH complex (17,22). Interestingly, the two subunits of TFIIH that interact with XPC/Rad4 (p62/Tfb1 and XPB/Ssl2) are also involved in recruiting XPG/Rad2 (23,24), and this suggests these two repair factors may form similar types of interactions with TFIIH that lead to their exchange during NER.

Despite the important role that the XPC/Rad4–TFIIH complex plays in regulating GG-NER, there is currently no detailed information describing the regions of XPC/Rad4 that interact with either the p62/Tfb1 or XPB/Ssl2 subunits of TFIIH. In this study, we characterize the interaction between Rad4 and the Tfb1 subunit of TFIIH. We identify an acidic segment from the N-terminal region of Rad4 (Rad4<sub>76–115</sub>; residues 76–115) that binds with high affinity to the PH domain located at the N-terminus of the Tfb1 subunit of TFIIH (Tfb1PH; residues 1–115). NMR spectroscopy studies show that Rad4<sub>76–115</sub> binds to the same region of Tfb1PH as two homologous acidic segments from Rad2, and Rad4<sub>76–115</sub> competes with these Rad2 segments for binding to Tfb1PH. Structural characterization of a Rad4<sub>76–115</sub>–Tfb1PH complex indicates that Rad4 binds to Tfb1PH using a very similar Tfb1PH-binding motif as Rad2 (25). In addition, *in vivo*

studies show that yeast with mutations of key residues of Rad4 required for interaction with Tfb1 display enhanced sensitivity to UV irradiation. Together these results provide a rationale for the role that TFIIH binding plays in the exchange between XPC/Rad4 and XPG/Rad2 during GG-NER.

## MATERIALS AND METHODS

### Strains, media and vectors

*Saccharomyces cerevisiae* strains used for these studies are listed in Supplementary Table S1. The strains were grown on a synthetic complete media (SC: 0.67% yeast nitrogen base without amino acids, 2% glucose and a mixture of amino acids and vitamins) lacking uracil (SC-U) for selection. All yeast transformations were performed using the modified lithium acetate protocol (26).

### Plasmid preparations

The pRS316RAD4cmyc plasmid (*RAD4*) was generated by amplification of the *RAD4* open reading frame (ORF) complemented by 190-bp upstream and 282-bp downstream on genomic DNA and insertion into pRS316. The pRS316RAD4(F95P/V98P)cmyc plasmid (*rad4-PP*) was obtained by using QuikChange II site-directed mutagenesis kit (Stratagene). The pRS316RAD4(W649A/L652A/L656A)cmyc (*rad4-AAA*) and pRS316RAD4(F95P/V98P/W649A/L652A/L656A)cmyc (*rad4-PPAAA*) plasmids were both obtained by overlapped PCR using either pRS316RAD4cmyc or pRS316RAD4(F95P/V98P)cmyc, respectively, as the cloning vector (For details see 'Supplementary Methods' section).

### Sensitivity assays

Yeast strains were grown overnight at 30°C in selective media. The next day they were diluted in order to obtain an OD<sub>595</sub> = 0.5–1 the following morning. The cells were then harvested by centrifugation, washed and resuspended in sterile water to obtain an OD<sub>595</sub> = 0.5. For UV-sensitivity assays, dilutions were plated on selective media (SC-U) and irradiated with UV light (XL-1000 UV crosslinker, SpectroLinker) at varying energy levels. The surviving colonies were counted after 3 days growth at 30°C, in the dark.

### Cloning and purification of proteins

The GST-Tfb1PH (residues 1–115 of Tfb1) was prepared as described (27). GST-Rad4<sub>76–115</sub> was prepared by inserting the appropriate region of Rad4 (Open Biosystems) into the pGEX-2T expression vector. GST-Rad34<sub>41–63</sub> was prepared by inserting the appropriate region of Rad34 (Open Biosystems) into the pGEX-2T expression vector. All point mutants were made using QuikChange II site-directed mutagenesis kit (Stratagene). All coding sequences were verified by DNA sequencing. Tfb1PH was purified as described (27). Rad4<sub>76–115</sub>, GST-Rad34<sub>41–63</sub> and their mutants were expressed as GST-fusion proteins in *Escherichia coli* host strain TOPP2, purified over GSH

resin (GE Healthcare) and cleaved with thrombin (Calbiochem), as previously described for Tfb1PH (27). Following cleavage with thrombin, the proteins were purified over a Q-Sepharose High Performance (GE Healthcare) column and dialyzed into appropriate buffers for isothermal titration calorimetry (ITC) and NMR studies.  $^{15}\text{N}$ -labeled and  $^{15}\text{N}/^{13}\text{C}$ -labeled proteins were prepared in M9-minimal media containing  $^{15}\text{NH}_4\text{Cl}$  (Sigma) and/or  $^{13}\text{C}_6$ -glucose (Sigma), as the sole nitrogen and carbon sources. For all experiments, protein concentrations were determined from  $A_{280}$ .

### ITC experiments

ITC titrations were performed as described (28) at 25°C in 20 mM sodium phosphate buffer (pH 7.5). All titrations fit a single-binding site mechanism with 1:1 stoichiometry and values are the average of two or more separate experiments.

### NMR experiments

The NMR chemical shift perturbation and competition experiments were performed as previously described (for sample details please see 'Supplementary Methods' section). For the NMR structural studies of the Rad<sub>476–115</sub>-Tfb1PH complex, four different samples containing 1.0 mM of the complex in a 1:1.25 ratio were used ( $^{15}\text{N}$ -Tfb1PH-Rad<sub>476–115</sub>,  $^{15}\text{N}/^{13}\text{C}$ -Tfb1PH-Rad<sub>476–115</sub>,  $^{15}\text{N}$ -Rad<sub>476–115</sub>-Tfb1PH and  $^{15}\text{N}/^{13}\text{C}$ -Rad<sub>476–115</sub>-Tfb1PH, respectively). All NMR experiments were carried out in 20 mM sodium phosphate (pH 6.5), 1 mM ethylenediaminetetraacetic acid, 1 mM DTT and 90% H<sub>2</sub>O/10% D<sub>2</sub>O or 100% D<sub>2</sub>O, at 300 K on Varian Unity Inova 500, 600 and 800 MHz spectrometers equipped with z-pulsed-field gradient units and triple resonance probes. All of the  $^1\text{H}$ ,  $^{15}\text{N}$  and  $^{13}\text{C}$  resonances for Rad<sub>476–115</sub> and Tfb1PH were assigned as reported for free Tfb1PH (29). Briefly, 3D HNCO (30), 3D HNCACB (31), 3D CBCACONH (32), 3D (H)C(CO)NH (33), 3D H(CCO)NH (33) and 3D HCCH-COSY (34) spectra were used to assign the backbone and aliphatic side chains resonances. The aromatic side chains  $^1\text{H}$ ,  $^{13}\text{C}$  and  $^{15}\text{N}$  resonances were assigned using a combination of 2D (HB)CB(CGCD)HD and 2D (HB)CB(CGCDCE)HE spectra (35). Interproton distance restraints were measured from 3D  $^{15}\text{N}$ -edited NOESY-HSQC,  $^{13}\text{C}$ -edited HMQC-NOESY ( $\tau_m = 90$  ms) and 3D  $^{15}\text{N}/^{13}\text{C}$  {F1}-filtered, {F3}-edited NOESY spectra ( $\tau_m = 90$  ms) (36,37). The NMR data were processed with NMRPipe/NMRDraw (38) and analyzed with NMRView (39) and Analysis from the CCPNMR suite (40).

### Structure calculations

The nuclear Overhauser effect-derived distance restraints (NOE) were divided. However, other NAR papers use NOE into four classes defined as strong (1.8–2.8 Å), medium (1.8–4.0 Å), weak (1.8–5.0 Å) and very weak (3.3–6.0 Å). Backbone dihedral angles were derived with the program TALOS+ (41). The structure of the Rad<sub>476–115</sub>-Tfb1PH complex was calculated using the program CNS (42). The quality of the structures was

analyzed with the programs PROCHECK-NMR (43) and MOLMOL (44). Ramachandran plot analysis showed that 76.9, 20.7, 1.5 and 0.9% of residues are in the most favored, additionally allowed, generously allowed and disallowed regions, respectively. The figures were generated with the program PyMol (Schrödinger).

## RESULTS

### The N-terminal segment of Rad4 binds Tfb1PH with high affinity

We previously identified two acidic segments within the spacer region of Rad2 (Rad<sub>2359–383</sub> and Rad<sub>2642–690</sub>) that contain a high-affinity Tfb1PH-binding motif (25). Based on the fact that XPC/Rad4 and XPG/Rad2 have been shown to be mutually exclusive in their binding to TFIID (20,21), we analyzed the sequences of Rad4 and XPC to see if they also contain a region similar to the Tfb1PH-binding motif found in Rad2. The requirements for the two Tfb1PH-binding motifs of Rad2 are that they are located within highly acidic segments and they contain an aromatic residue (W or F) followed by two acidic residues and a valine residue. As shown in Figure 1a, sequences similar to the Tfb1PH-binding motifs of Rad2 are located near the N-terminus of both Rad4 (residues 86–106) and XPC (residues 124–144). This observation is consistent with the first 167 amino acids of Rad4 being sufficient for binding to TFIID and the fact that the p62/Tfb1 subunit of TFIID has been shown to directly interact with XPC/Rad4 (9,17,22).

To determine whether the N-terminal region of Rad4 does in fact bind to Tfb1PH, the apparent dissociation constant ( $K_d$ ) between Tfb1PH and Rad<sub>476–115</sub> was measured by ITC (Figure 1b and c). As we observed with Rad<sub>2359–383</sub> and Rad<sub>2642–690</sub> ( $K_d = 130$  nM and  $K_d = 190$  nM, respectively), Rad<sub>476–115</sub> binds to Tfb1PH with high affinity ( $K_d = 50$  nM). Next, we wanted to verify that Phe95 and Val98 of Rad4 were crucial residues in the Tfb1PH-binding motif of Rad4. These residues correspond to Phe670 and Val673 of Rad<sub>2642–690</sub> and are crucial for Rad2 binding to Tfb1PH (25). Mutation of either Phe95 or Val98 to proline (F95P and V98P) reduces the affinity of Rad<sub>476–115</sub> for Tfb1PH by 50- and 24-fold, respectively (Figure 1b), supporting that the Tfb1PH-binding site of Rad4 is very similar to the two sites found in Rad2.

### Rad<sub>476–115</sub>, Rad<sub>2359–383</sub> and Rad<sub>2642–690</sub> bind a common site on Tfb1PH

To identify the binding site of Rad<sub>476–115</sub> on Tfb1PH, NMR chemical shift perturbation studies were performed. In these experiments, addition of unlabeled Rad<sub>476–115</sub> to  $^{15}\text{N}$ -labeled Tfb1PH causes significant changes in the  $^1\text{H}$  and  $^{15}\text{N}$  chemical shifts for several Tfb1PH signals in the  $^1\text{H}$ - $^{15}\text{N}$  HSQC spectra (Supplementary Figure S1a and b). When mapped onto the structure of Tfb1PH, the residues exhibiting significant changes are located in strands  $\beta 5$ ,  $\beta 6$ ,  $\beta 7$  and helix H1 (Figure 2a). The residues experiencing significant changes are almost identical to those observed when either of the two acidic segments from

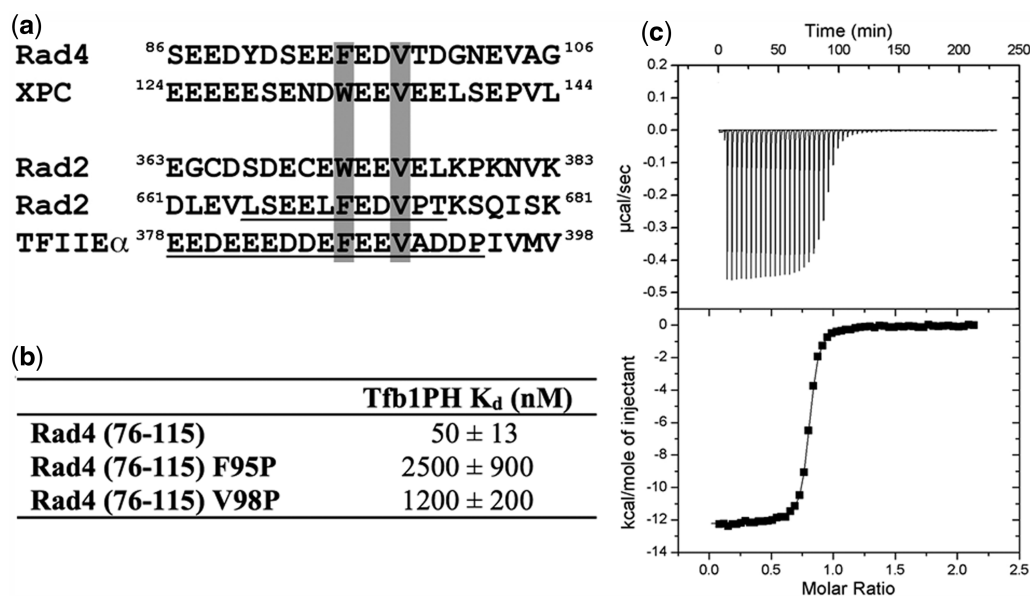


**Figure 1.** The N-terminal region of Rad4 contains a high-affinity Tfb1PH-binding site. (a) Identification of an amino acid segment located between residues 86 and 106 of Rad4 that aligns with the Tfb1PH-binding motif found in Rad2 and TFIIIE $\alpha$ CTD. A similar motif is also located between residues 124 and 144 of XPC. In these alignments, the residues of TFIIIE $\alpha$ CTD and Rad2<sub>642-690</sub> that form the binding interface with p62PH/Tfb1PH are underlined and crucial hydrophobic residues are shaded in gray. (b) Comparison of the dissociation constant ( $K_d$ ) values for the binding of Rad4<sub>76-115</sub> and its mutants (F95P and V98P) to Tfb1PH. (c) Thermogram of the Tfb1PH titration with successive additions of Rad4<sub>76-115</sub>. Experiments are performed at 25°C, in 20 mM NaPO<sub>4</sub> pH 7.5 buffer, and the results fit to a single-binding site model with 1:1 stoichiometry.

Rad2 (Rad2<sub>359-383</sub> and Rad2<sub>642-690</sub>) bind to Tfb1PH (Figure 2b and Supplementary Figure S1c).

To confirm that Rad4<sub>76-115</sub> shares a common binding site on Tfb1PH with Rad2<sub>359-383</sub>, NMR competition experiments were performed. In these experiments, we first add a substoichiometric concentration of unlabeled Tfb1PH (0.4 mM) to a sample containing <sup>15</sup>N-labeled Rad4<sub>76-115</sub> (0.5 mM) and as expected, we observe significant changes for several <sup>1</sup>H and <sup>15</sup>N chemical shifts in the <sup>1</sup>H-<sup>15</sup>N HSQC spectra of Rad4<sub>76-115</sub> (Figure 2c). We then add an equimolar amount of unlabeled Rad2<sub>359-383</sub> (0.5 mM) to the <sup>15</sup>N-Rad4<sub>76-115</sub>-Tfb1PH complex and observe that the <sup>1</sup>H and <sup>15</sup>N resonances of Rad4<sub>76-115</sub>, which shift upon formation of the Rad4<sub>76-115</sub>-Tfb1PH complex return to values characteristic of the free form of Rad4<sub>76-115</sub> (Figure 2d). Taken together with previous results showing that Rad2<sub>359-383</sub> and Rad2<sub>642-690</sub> compete for binding to Tfb1PH (25), these results demonstrate that Rad4<sub>76-115</sub>, Rad2<sub>359-383</sub> and Rad2<sub>642-690</sub> all compete for a common binding site on Tfb1PH.

#### The Rad4 homolog Rad34 also contains a Tfb1PH-binding motif

Rad34 is a repair factor found in yeast that plays a role similar to Rad4 in TC-NER of ribosomal DNA (rDNA) (45,46). Given the fact that TFIIH also plays a critical role in RNA polymerase I (RNAP I)-dependent transcription and TC-NER of rDNA (47), we were interested to determine whether Rad34 also contained a Tfb1PH-binding motif. The Rad34 protein is homologous to the Rad4 protein, and it contains both a DNA-binding domain that recognizes damaged DNA and a TFIIH/

Centrin-2-binding motif within its C-terminal region (48). Although there is currently no evidence that Rad34 interacts with TFIIH, we postulated based on its homology to Rad4, that it also contains a Tfb1PH-binding motif near the N-terminus of the protein. Based on sequence homology with Rad4<sub>75-116</sub>, we identified a segment between residues 41 and 63 of Rad34 (Rad34<sub>41-63</sub>; Figure 3a) as a potential Tfb1PH-binding motif, since it contains a highly acidic stretch that includes an aromatic residue (Trp54) followed by two acidic residues and a valine (Val57). ITC studies show that Rad34<sub>41-63</sub> also binds to Tfb1PH with high affinity ( $K_d = 11.0$  nM; Figure 3b) and that mutation of Trp54 to a serine (W54S mutant) significantly reduces binding to Tfb1PH (over three orders of magnitude). To further define the mode of binding of Rad34<sub>41-63</sub> to Tfb1PH, an NMR chemical shift perturbation study was performed. Like for Rad4<sub>76-115</sub>, addition of Rad34<sub>41-63</sub> to <sup>15</sup>N-Tfb1PH causes significant changes in the <sup>1</sup>H and <sup>15</sup>N chemical shifts for several Tfb1PH signals in the <sup>1</sup>H-<sup>15</sup>N HSQC spectra (Supplementary Figure S2) and the residues exhibiting significant changes are located in strands  $\beta$ 5,  $\beta$ 6,  $\beta$ 7 and the H1 helix (Figure 3c).

#### The two TFIIH-binding regions of Rad4 are crucial to survival following UV irradiation

Previous studies have shown that both the N- and C-terminal regions of XPC/Rad4 interact with TFIIH (9,14-17). To examine the functional role of these two TFIIH-binding regions of Rad4 in yeast survival following exposure to UV irradiation, we first prepared a yeast strain in which the two key hydrophobic residues (Phe95

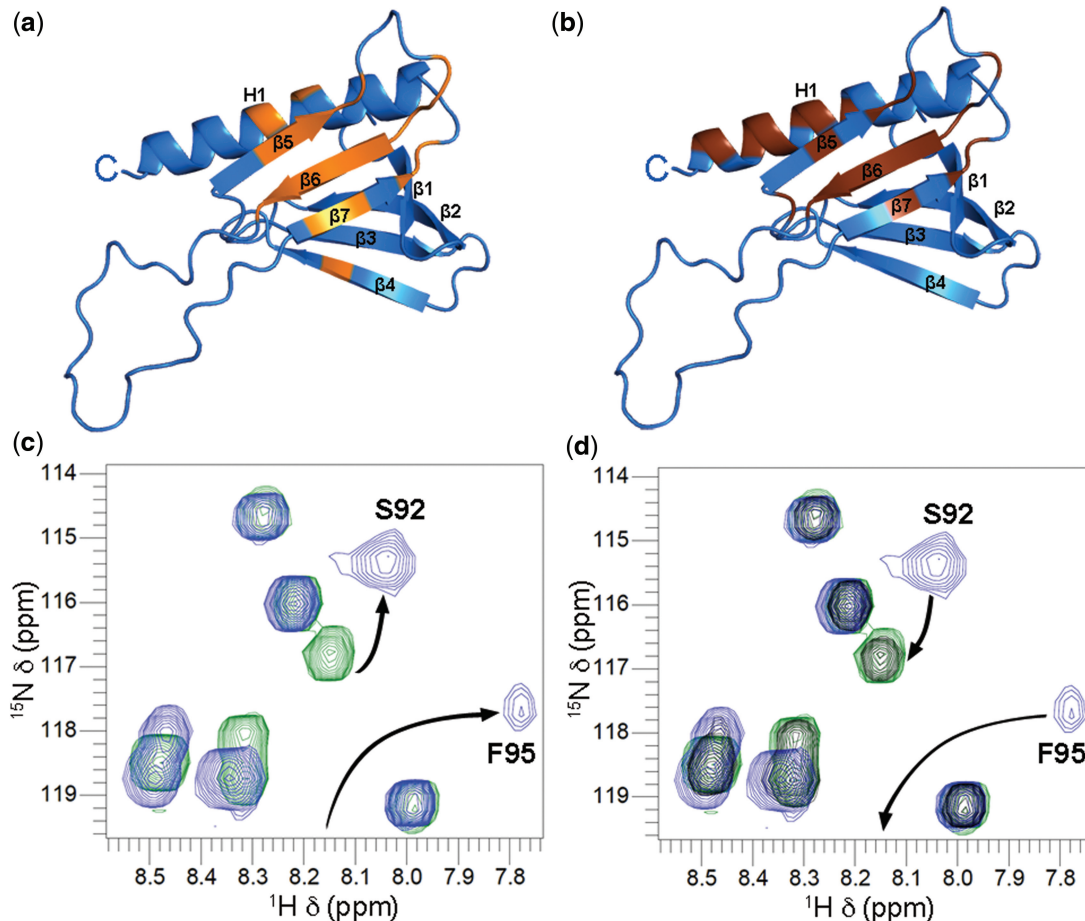


**Figure 2.** Rad4<sub>76-115</sub> and Rad2<sub>359-383</sub> share a common binding site on Tfb1PH. (a and b) Ribbon model of the 3D structure of Tfb1PH (blue; PDB code 1Y5O). The amino acids of Tfb1PH showing a significant chemical shift change  $\{\Delta\delta(\text{ppm}) > 0.15; \Delta\delta = [(0.17\Delta N_H)^2 + (\Delta H_N)^2]^{1/2}\}$  upon formation of a complex with either Rad4<sub>76-115</sub> (a) or Rad2<sub>359-383</sub> (b) are highlighted in orange and brown, respectively. (c) Overlay of a selected region from the <sup>1</sup>H-<sup>15</sup>N HSQC spectra of <sup>15</sup>N-labeled Rad4<sub>76-115</sub> (0.5 mM) in the free form (green) and in the presence of unlabeled Tfb1PH (0.4 mM; blue). (d) Same overlay as in (c), but after the addition of unlabeled Rad2<sub>359-383</sub> (1.5 mM; black). Rad4<sub>76-115</sub> signals that undergo significant changes in <sup>1</sup>H and <sup>15</sup>N chemical shifts upon formation of the complex with Tfb1PH (c), and return towards their original position following the addition of Rad2<sub>359-383</sub> (d) are indicated by arrows.

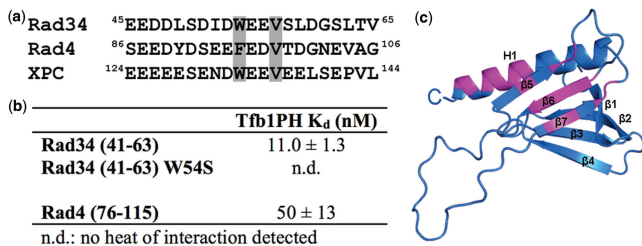


**Figure 3.** Rad34 contains a Tfb1PH-binding motif. (a) Identification of an amino acid segment located between residues 41 and 63 from Rad34 that aligns with the Tfb1PH-binding motif from Rad4 and XPC. The two crucial hydrophobic residues in the motif are shaded in gray. (b) Comparison of the dissociation constant ( $K_d$ ) values for the binding of Rad4<sub>76-115</sub> and Rad34<sub>41-63</sub> with Tfb1PH. No binding is observed with the W54S mutant of Rad34<sub>41-63</sub> under the experimental conditions indicating a  $K_d > 10 \mu\text{M}$ . (c) Ribbon model of the 3D structure of Tfb1PH (blue). The amino acids of <sup>15</sup>N-labeled Tfb1PH showing a significant chemical shift change  $\{\Delta\delta(\text{ppm}) > 0.15; \Delta\delta = [(0.17\Delta N_H)^2 + (\Delta H_N)^2]^{1/2}\}$  upon formation of a complex with Rad34<sub>41-63</sub> are highlighted in magenta.

and Val98) in the Tfb1PH-binding motif) were mutated to proline (*rad4-PP*) and we tested it for survival following exposure to UV irradiation. The *rad4-PP* strain shows only a slightly enhanced sensitivity to UV irradiation when compared with the wild-type *RAD4* strain (Figure 4a). Next, we tested the role of the C-terminal TFIIF-binding motif of Rad4. Previous studies have shown that mutating three key hydrophobic residues (Trp649, Leu652 and Leu656) in this region to alanine leads to yeast strains (*rad4-AAA*) with enhanced sensitivity to UV irradiation as well as decreased binding to TFIIF and Centrin-2 (15). Consistent with previous studies, the *rad4-AAA* mutant strain is more sensitive to UV irradiation than the *RAD4* strain as well as slightly more sensitive than the *rad4-PP* strain (Figure 4a).

To further examine the *in vivo* role of the two TFIIF-binding regions of Rad4, the N-terminal mutation (*rad4-PP*) and the C-terminal mutation (*rad4-AAA*) were combined to produce an additional mutant strain (*rad4-PPAAA*). The survival curves show that the *rad4-PPAAA* strain is considerably more sensitive to UV irradiation

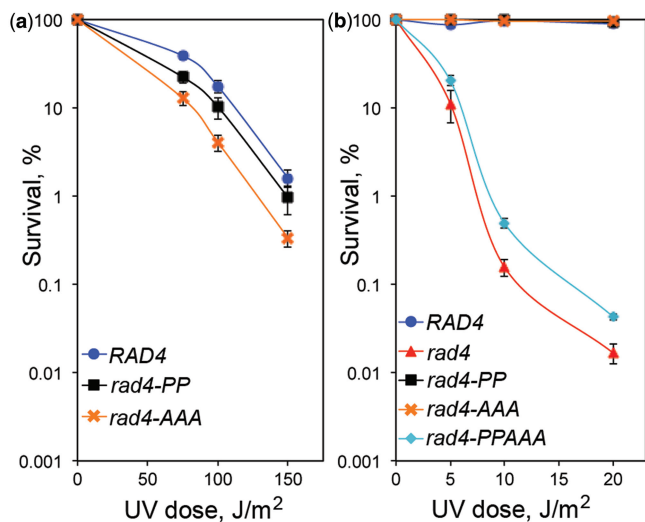


**Figure 4.** The two TFIIH-binding regions of Rad4 are crucial for survival following UV irradiation. (a) The survival of *RAD4* (blue), *rad4-PP* (black) and *rad4-AAA* yeast were determined following increasing doses of UV irradiation. (b) The survival of *RAD4* (blue), *rad4* (red), *rad4-PP* (black), *rad4-AAA* (orange) and *rad4-PPAAA* (aqua) yeast were determined following increasing doses of UV irradiation. In both (a) and (b), the y-axis represents the percentage of surviving cells (normalized to the number of viable cells not exposed to UV light) and the x-axis shows the energy levels of the UV irradiation applied ( $\text{J/m}^2$ ). The results are the mean  $\pm$  SEM of three independent experiments.

than either the *rad4-PP* or *rad4-AAA* strains and displays similar sensitivity to what is observed with the *rad4* deletion strain (Figure 4b). This increased sensitivity to UV irradiation is not the result of decreased levels of Rad4 as the Rad4-PPAAA mutant protein is expressed at similar levels as the wild-type Rad4 (Supplementary Figure S3). Taken together, the *in vivo* studies in yeast indicate that the Tfb1PH-binding motif of Rad4 plays a key role in yeast survival following exposure to UV irradiation. In addition, mutating both of the known TFIIH-binding regions of Rad4 produces a dramatic effect on yeast sensitivity to UV irradiation, suggesting that at least two distinct interactions occur between Rad4 and TFIIH and that these interactions appear to be almost redundant for Rad4 function in DNA repair.

#### NMR structure determination of the Rad4<sub>76–115</sub>–Tfb1PH complex

To compare Rad2 and Rad4 in complex with Tfb1PH, we determined the NMR solution structure of a Rad4<sub>76–115</sub>–Tfb1PH complex. The structure of the Rad4<sub>76–115</sub>–Tfb1PH complex (PDB code 2M14) is well defined by the NMR data (Table 1). The 20 lowest energy structures (Figure 5a) are characterized by good backbone geometry, no significant restraint violation and low pair-wise r.m.s.d. values (Table 1). As is the case for the Rad2<sub>642–690</sub>–Tfb1PH complex, the structure of Tfb1PH in complex with Rad4<sub>76–115</sub> is virtually identical to its free form showing a typical PH domain fold consisting of a seven-stranded  $\beta$ -sandwich ( $\beta$ 1– $\beta$ 7) flanked on one side by a long  $\alpha$ -helix (H1) (27). In complex with Tfb1PH,

**Table 1.** NMR and refinement statistics for Rad4 in complex with Tfb1PH<sup>a</sup>

NMR distance and dihedral constraints	
Distance constraints	
Total NOE	1599
Intra-residue	556
Inter-residue	
Sequential ( $ i-j  = 1$ )	359
Medium-range ( $ i-j  < 4$ )	200
Long-range ( $ i-j  > 5$ )	484
Intermolecular	28
Hydrogen bonds	36
Total dihedral angle restraints	148
$\phi$	74
$\psi$	74
Structure statistics	
Violations (mean and SD)	
Distance constraints (Å)	$0.0179 \pm 0.0006$
Dihedral angle constraints (°)	$0.18 \pm 0.03$
Max. dihedral angle violation (°)	5
Max. distance constraint violation (Å)	0.5
Deviations from idealized geometry	
Bond lengths (Å)	$0.00210 \pm 0.00007$
Bond angles (°)	$0.376 \pm 0.004$
Improvers (°)	$0.209 \pm 0.008$
Average pairwise r.m.s. deviation (Å) <sup>b</sup>	
Heavy	$1.31 \pm 0.12$
Backbone	$0.67 \pm 0.14$

<sup>a</sup>The 20 conformers with the lowest energies were selected for statistical analysis.

<sup>b</sup>Only residues 5–63 and 86–112 of Tfb1PH and residues 95–99 of Rad4 were used for the r.m.s.d. calculations. Residues at the N-terminus (1–4), at the C-terminus (113–115), and in the flexible loop (64–85) of Tfb1PH, as well as residues at the N-terminus (76–94) and at the C-terminus (100–115) of Rad4 were not included in the calculation.

Rad4<sub>76–115</sub> binds in an extended conformation devoid of any regular secondary structural element with residues 95–98 forming a crucial portion of the interface with Tfb1PH. This is consistent with the <sup>1</sup>H–<sup>15</sup>N HSQC spectra of the titration of <sup>15</sup>N-labeled Rad4<sub>76–115</sub> with Tfb1PH as residues 95–98 undergo the most significant changes in both their <sup>1</sup>H and <sup>15</sup>N chemical shifts (Supplementary Figure S4).

#### Rad4<sub>76–115</sub>–Tfb1PH-binding interface

In the complex, Rad4<sub>76–115</sub> binds in an extended form to two adjacent shallow grooves on the surface of Tfb1PH. The first groove is formed by residues Gln49, Ala50, Thr51, Pro52, Met59, Leu60, Arg61 and Met88 from strands  $\beta$ 5,  $\beta$ 6 and  $\beta$ 7 of Tfb1PH (Figure 5b). Phe95 of Rad4 inserts into this groove where it is in position to form a cation– $\pi$  interaction with Arg61. The second groove is composed of Leu48, Ala50, Lys101 and Gln105, Ile108, Lys112 of Tfb1PH and accommodates Val98 and Thr99 of Rad4 (Figure 5c). Val98 is anchored on one side of this pocket through van der Waals interactions with both its methyl groups. Thr99 is anchored on the other side of the pocket through van der Waals interactions with its methyl group. Although the majority of the interactions within the two grooves are van der Waals contacts, an extensive series of positively charged residues on the surface of Tfb1PH (Lys47, Lys57, Arg61,

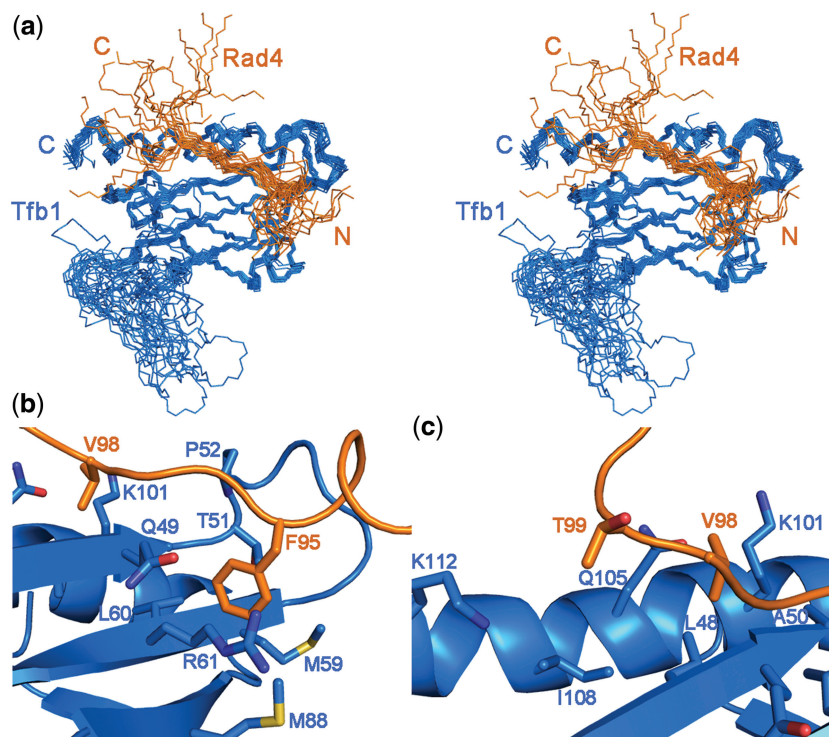


**Figure 5.** NMR structure of the Rad4<sub>76-115</sub>-Tfb1PH complex. (a) Stereo view of the 20 lowest-energy structures of the complex between Tfb1PH (blue) and Rad4<sub>76-115</sub> (orange; PDB code 2M14). The 3D structures were superimposed using the backbone atoms C', C<sup>α</sup> and N of residues 4–65 and 85–112 of Tfb1PH and residues 90–104 of Rad4<sub>76-115</sub>. (b) Ribbon representation of Tfb1PH (blue) and backbone trace of the region of Rad4<sub>76-115</sub> (orange) interacting in the first binding pocket. In this pocket, Phe95 of Rad4 forms a cation-π interaction with Arg61 of Tfb1 and van der Waals interactions with Met59. (c) Ribbon representation of Tfb1PH (blue) and backbone trace of the region of Rad4<sub>76-115</sub> (orange) interacting in the second binding pocket. On one side of the pocket Val98 of Rad4 interacts with Leu48, Ala50, Lys101 and Gln105 of Tfb1. On the other side of the pocket Thr99 of Rad4 interacts with Gln105, Ile108 and Lys112 of Tfb1.

Arg86, Lys101 and Lys112) surround the two grooves, where they function to position the negatively charged Rad4<sub>76-115</sub> (Supplementary Figure S5). The NMR structures support the formation of one potential salt bridge between Asp97 of Rad4<sub>76-115</sub> and Lys47 of Tfb1PH.

#### Comparison of the Rad4<sub>76-115</sub>-Tfb1PH and Rad2<sub>642-690</sub>-Tfb1PH interfaces

The structure of the Rad4<sub>76-115</sub>-Tfb1PH interface is virtually identical to the structure of the Rad2<sub>642-690</sub>-Tfb1PH interface (Figure 6). In both structures, a phenylalanine (Phe95 in Rad4 and Phe670 in Rad2) binds in a first pocket, where it is in position to make a cation-π interaction with Arg61 of Tfb1PH, or the analogous Gln64 in p62PH. In addition, a valine (Val98 in Rad4 and Val673 in Rad2) inserts into a second pocket, where it makes van der Waals contacts with a series of residues in Tfb1PH. Rad4 and Rad2 also contain a threonine (Thr99 in Rad4 and Thr675 in Rad2) that forms van der Waals contacts in the second binding pocket. In Rad2<sub>642-690</sub>, Val673 and Thr675 are separated by Pro674, whereas in Rad4<sub>76-115</sub>, Val98 and Thr99 are consecutive residues. In Rad2<sub>642-690</sub>, Pro674 creates a slight bend in the backbone so that the side-chains of Val673 and Thr675 can both be oriented towards the surface of Tfb1PH. One other important commonality between the two structures is that Rad4<sub>76-115</sub> and Rad2<sub>642-690</sub> both contain several acidic

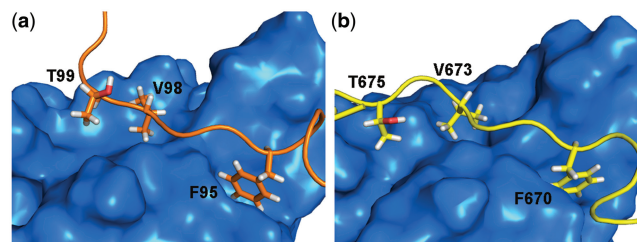


**Figure 6.** The interfaces of Rad2-Tfb1PH and Rad4-Tfb1PH complexes are very similar. The 3D structures of Tfb1PH are shown as molecular surfaces (blue) and Rad4<sub>76-115</sub> (a; orange), Rad2<sub>642-690</sub> (b; yellow) are shown as ribbons. Selected residues in the Tfb1PH-binding motif of Rad4<sub>76-115</sub> and Rad2<sub>642-690</sub> are also shown to demonstrate the similarity between their binding interfaces.

residues that participate in electrostatic interactions with basic amino acids that surround the perimeter of the two binding pockets of Tfb1PH. Overall, the similarities between these two interfaces provide a structural framework to understand how Rad4 and Rad2 can compete for binding to Tfb1 in NER.

#### DISCUSSION

Following DNA damage recognition, the recruitment of TFIIH by XPC/Rad4 to the repair complex occurs

through direct interactions with its p62/Tfb1 and XPB/Ssl2 subunits (17,22). Once at the damaged DNA, TFIIH recruits XPG/Rad2 through direct interactions with multiple subunits including both the p62/Tfb1 and XPB/Ssl2 subunits (23,24). Given that XPC/Rad4 and XPG/Rad2 interact with the same subunits of TFIIH and appear to be mutually exclusive within the repair complex (10,20), XPG/Rad2 likely displaces XPC/Rad4 from the pre-incision complex in part by competing for common binding sites on the various subunits of TFIIH (Supplementary Figure S6). Thus, the competition observed for regions of Rad4 and Rad2 binding to Tfb1PH by NMR and the remarkable similarity between the structures of the Rad4<sub>76-115</sub>-Tfb1PH and Rad2<sub>642-690</sub>-Tfb1PH interfaces provides a molecular mechanism to rationalize the mutual exclusivity observed between XPC/Rad4 and XPG/Rad2 at the repair complex *in vivo*. Although a hand-off or displacement mechanism has previously been suggested between XPC/Rad4 and XPG/Rad2 in NER (49), this is the first structural evidence to support such a displacement mechanism.

This displacement of XPC/Rad4 by XPG/Rad2 could serve at least two possible purposes for maintaining the NER complex in a repair-competent form. First, it assures that TFIIH is always stabilized on the DNA and available for repair as opposed to being recruited to perform alternative functions such as transcription. Second, it helps to establish the correct orientation of XPG/Rad2 on the DNA lesion. XPG/Rad2 cleaves the phosphate backbone of DNA on the 3'-side of the lesion, and it is crucial that this is done in a precise fashion for NER to be carried out in an accurate manner. Since XPC/Rad4 specifically interacts on the same side of the damaged DNA (12), a sequential displacement mechanism would serve to place XPG/Rad2 in the correct orientation for precise repair of the DNA lesion without the need for release of TFIIH. This model is similar to the 'passing the baton' mechanism seen in base excision repair (BER) (50). In the BER model, the substrate is channeled from one protein to another as opposed to a pre-formed protein complex that possesses all the activities necessary for repair.

The fact that both the N-terminal Tfb1PH-binding motif and the C-terminal TFIIH/Centrin-2-binding region of Rad4 play a role in yeast survival following exposure to UV irradiation is consistent with the sequential displacement mechanism between XPC/Rad4 and XPG/Rad2 in NER. In the case of XPG/Rad2, it has also been shown to interact with multiple subunits of TFIIH, including p62/Tfb1 and XPB/Ssl2, by participating in a series of weak interactions with its extended spacer region (23,51,52). Similarly, XPC/Rad4 has been shown to directly interact with both the p62/Tfb1 and XPB/Ssl2 subunits of TFIIH through regions in both termini of the protein (10,20) and our *in vivo* results in yeast support the importance of both these regions. The fact that a mutation of the C-terminal region of Rad4 has a slightly larger effect on yeast survival following UV irradiation than a mutation of the N-terminal region, is consistent with previous results showing that the C-terminal region of XPC appeared critical for TFIIH binding (17). Taken together with our current results,

this indicates that although displacement of both the N-terminal and the C-terminal region of XPC/Rad4 by XPG/Rad2 is important for NER, the displacement of the C-terminal region may be the rate-limiting step. However, the details of the interaction between the C-terminal region of Rad4 and TFIIH are currently unknown and it is still not clear in which order the displacement of the two regions of XPC/Rad4 occurs.

The sequential displacement mechanism clearly presents advantages for maintaining the integrity and accuracy of the repair complex; however, it may also be important for sequestering TFIIH. We have previously shown that the Rad2<sub>642-690</sub>-Tfb1PH interface is similar to the interface formed in a complex between the C-terminal domain of TFIIIE $\alpha$  (TFIIIE $\alpha$ CTD) and p62PH (25,53). Like Rad4 and Rad2, TFIIIE $\alpha$ CTD contains a Tfb1PH-binding motif that consists of an aromatic residue followed by two acidic residues and a valine (54). We previously suggested that the similarity of the Tfb1PH-binding motif in Rad2 and TFIIIE $\alpha$  provides a mechanistic link between the role of TFIIH in transcription and repair. Our current work further strengthens this concept since a highly similar Tfb1PH-binding motif is present in XPC, Rad4 and Rad34. TFIIH plays an important role both in RNAP I-dependent transcription as well as in NER of rDNA (47), and Rad34 likely forms a similar interaction with Tfb1 that may regulate RNAP I-associated NER. Based on the structural similarities of the Rad4<sub>76-115</sub>-Tfb1PH, Rad2<sub>642-690</sub>-Tfb1PH and the TFIIIE $\alpha$ CTD-p62PH interfaces, it is tempting to propose that the interplay of TFIIIE $\alpha$ , Rad4 and Rad2 interacting with p62/Tfb1 helps to determine whether TFIIH is functioning in transcription or repair. In RNAP II-dependent transcription, TFIIIE $\alpha$ CTD recruits TFIIH to the pre-initiation complex (PIC) through interactions with the p62/Tfb1 subunit of TFIIH (54). Once at the PIC, TFIIH serves multiple functions during transcription by virtue of its helicase (XPB/Ssl2 and XPD/Rad3) and kinase (Cdk7/Kin28) activities (55,56). During NER, TFIIH's role in transcription would be limited by its recruitment to the DNA lesion through interactions with Rad4 that involves in part the same p62/Tfb1 subunit. As repair progresses past the initial recognition of the DNA lesion to the incision steps, TFIIH remains associated with the repair complex through interactions with XPG/Rad2. This would make the process more efficient since it would help to prevent TFIIH being recruited for transcription.

In conclusion, we provide the first structural evidence for the displacement mechanism between XPC/Rad4 and XPG/Rad2 during NER. Our data shows that XPC/Rad4 and XPG/Rad2 form similar interactions with the p62/Tfb1 subunit of TFIIH, and this supports the hypothesis that XPG/Rad2 displaces XPC/Rad4 from the repair complex through a series of interactions with different subunits of TFIIH. In addition, the structure of the Rad4<sub>76-115</sub>-Tfb1PH complex provides a common mechanistic explanation for the recruitment of TFIIH to both the PIC and the NER complex. Future studies are needed to determine if other subunits of TFIIH, in particular XPB/Ssl2, also form similar interactions with XPC/Rad4

and XPG/Rad2, and what roles they play in the displacement of XPC/Rad4 by XPG/Rad2.

## ACCESSION NUMBERS

2M14.

## SUPPLEMENTARY DATA

Supplementary Data are available at NAR Online: Supplementary Tables 1 and 2, Supplementary Figures 1–6, Supplementary Methods and Supplementary Reference [57].

## ACKNOWLEDGEMENTS

The authors would like to thank Aurélie Bernier and Antoine Chiasson for help with protein purification and Dr Tara Sprules for assistance with several NMR experiments.

## FUNDING

The Canadian Cancer Society (J.G.O.). J.L.-V. is a Vanier Canada Graduate Scholar from the Canadian Institutes of Health Research. L.C. is a postdoctoral fellow of the Natural Sciences and Engineering Research Council of Canada CREATE program. P.L. is a Canadian Research Chair in Structural Biology and Engineering of RNA. 800 MHz NMR experiments were recorded at the Québec/Eastern Canada High Field NMR Facility, supported by the Natural Sciences and Engineering Research Council of Canada. Funding for open access charge: Canadian Cancer Society.

*Conflict of interest statement.* None declared.

## REFERENCES

- Friedberg, E.C., Walker, G.C., Siede, W., Wood, R.D., Schultz, T. and Ellenberger, T. (2005) *DNA Repair and Mutagenesis*. ASM Press, Washington, DC.
- Lehmann, A.R. (2003) DNA repair-deficient diseases, xeroderma pigmentosum, Cockayne syndrome and trichothiodystrophy. *Biochimie*, **85**, 1101–1111.
- Cartault, F., Nava, C., Malbrunot, A.C., Munier, P., Hebert, J.C., N'Guyen, P., Djeridi, N., Pariaud, P., Pariaud, J., Dupuy, A. *et al.* (2011) A new XPC gene splicing mutation has led to the highest worldwide prevalence of xeroderma pigmentosum in black Mahori patients. *DNA Repair*, **10**, 577–585.
- Hoeymakers, J.H. (2001) Genome maintenance mechanisms for preventing cancer. *Nature*, **411**, 366–374.
- Sugasawa, K., Ng, J.M., Masutani, C., Iwai, S., van der Spek, P.J., Eker, A.P., Hanaoka, F., Bootsma, D. and Hoeymakers, J.H. (1998) Xeroderma pigmentosum group C protein complex is the initiator of global genome nucleotide excision repair. *Mol. Cell*, **2**, 223–232.
- Fitch, M.E., Nakajima, S., Yasui, A. and Ford, J.M. (2003) In vivo recruitment of XPC to UV-induced cyclobutane pyrimidine dimers by the DDB2 gene product. *J. Biol. Chem.*, **278**, 46906–46910.
- Tantin, D., Kansal, A. and Carey, M. (1997) Recruitment of the putative transcription-repair coupling factor CSB/ERCC6 to RNA polymerase II elongation complexes. *Mol. Cell Biol.*, **17**, 6803–6814.
- Sarker, A.H., Tsutakawa, S.E., Kostek, S., Ng, C., Shin, D.S., Peris, M., Campeau, E., Tainer, J.A., Nogales, E. and Cooper, P.K. (2005) Recognition of RNA polymerase II and transcription bubbles by XPG, CSB, and TFIIH: insights for transcription-coupled repair and Cockayne syndrome. *Mol. Cell*, **20**, 187–198.
- Bardwell, A.J., Bardwell, L., Iyer, N., Svejstrup, J.Q., Feaver, W.J., Kornberg, R.D. and Friedberg, E.C. (1994) Yeast nucleotide excision repair proteins Rad2 and Rad4 interact with RNA polymerase II basal transcription factor b (TFIIH). *Mol. Cell Biol.*, **14**, 3569–3576.
- Araujo, S.J., Nigg, E.A. and Wood, R.D. (2001) Strong functional interactions of TFIIH with XPC and XPG in human DNA nucleotide excision repair, without a preassembled repairosome. *Mol. Cell Biol.*, **21**, 2281–2291.
- Yokoi, M., Masutani, C., Maekawa, T., Sugawara, K., Ohkuma, Y. and Hanaoka, F. (2000) The xeroderma pigmentosum group C protein complex XPC-HR23B plays an important role in the recruitment of transcription factor IIIH to damaged DNA. *J. Biol. Chem.*, **275**, 9870–9875.
- Min, J.-H. and Pavletich, N.P. (2007) Recognition of DNA damage by the Rad4 nucleotide excision repair protein. *Nature*, **449**, 570–575.
- Miron, S., Duchambon, P., Blouquit, Y., Durand, D. and Craescu, C.T. (2008) The carboxy-terminal domain of xeroderma pigmentosum complementation group C protein, involved in TFIIH and centrin binding, is highly disordered. *Biochemistry*, **47**, 1403–1413.
- Chen, L. and Madura, K. (2008) Centrin/Cdc31 is a novel regulator of protein degradation. *Mol. Cell Biol.*, **28**, 1829–1840.
- den Dulk, B., van Eijk, P., de Ruijter, M., Brandsma, J.A. and Brouwer, J. (2008) The NER protein Rad33 shows functional homology to human Centrin2 and is involved in modification of Rad4. *DNA Repair*, **7**, 858–868.
- Popescu, A., Miron, S., Blouquit, Y., Duchambon, P., Christova, P. and Craescu, C.T. (2003) Xeroderma pigmentosum group C protein possesses a high affinity binding site to human centrin 2 and calmodulin. *J. Biol. Chem.*, **278**, 40252–40261.
- Uchida, A., Sugawara, K., Masutani, C., Dohmae, N., Araki, M., Yokoi, M., Ohkuma, Y. and Hanaoka, F. (2002) The carboxy-terminal domain of the XPC protein plays a crucial role in nucleotide excision repair through interactions with transcription factor IIIH. *DNA Repair*, **1**, 449–461.
- Coin, F., Oksenyich, V. and Egly, J.-M. (2007) Distinct roles for the XPB/p52 and XPD/p44 subcomplexes of TFIIH in damaged DNA opening during nucleotide excision repair. *Mol. Cell*, **26**, 245–256.
- Schärer, O.D. (2008) The molecular basis for different disease states caused by mutations in TFIIH and XPG. *DNA Repair*, **7**, 339–344.
- Riedl, T., Hanaoka, F. and Egly, J.M. (2003) The comings and goings of nucleotide excision repair factors on damaged DNA. *EMBO J.*, **22**, 5293–5303.
- Wakasugi, M. and Sancar, A. (1998) Assembly, subunit composition, and footprint of human DNA repair excision nuclease. *Proc. Natl Acad. Sci. USA*, **95**, 6669–6674.
- Bernardes de Jesus, B.M., Bjaras, M., Coin, F. and Egly, J.M. (2008) Dissection of the molecular defects caused by pathogenic mutations in the DNA repair factor XPC. *Mol. Cell Biol.*, **28**, 7225–7235.
- Hohl, M., Dunand-Sauthier, I., Staresinic, L., Jaquier-Gubler, P., Thorel, F., Modesti, M., Clarkson, S.G. and Schärer, O.D. (2007) Domain swapping between FEN-1 and XPG defines regions in XPG that mediate nucleotide excision repair activity and substrate specificity. *Nucleic Acids Res.*, **35**, 3053–3063.
- Iyer, N., Reagan, M.S., Wu, K.J., Canagarajah, B. and Friedberg, E.C. (1996) Interactions involving the human RNA polymerase II transcription/nucleotide excision repair complex TFIIH, the nucleotide excision repair protein XPG, and Cockayne syndrome group B (CSB) protein. *Biochemistry*, **35**, 2157–2167.
- Lafrance-Vanasse, J., Arseneault, G., Cappadocia, L., Chen, H.T., Legault, P. and Omichinski, J.G. (2012) Structural and functional characterization of interactions involving the Tfb1 subunit of TFIIH and the NER factor Rad2. *Nucleic Acids Res.*, **40**, 5739–5750.

26. Kaiser, C., Michaelis, S. and Mitchell, A. (1994) *Methods in Yeast Genetics*. Cold Spring Harbor Laboratory Press, Cold Spring Harbor, NY.
27. Di Lello, P., Nguyen, B.D., Jones, T.N., Potempa, K., Kobor, M.S., Legault, P. and Omichinski, J.G. (2005) NMR structure of the amino-terminal domain from the Tfb1 subunit of TFIID and characterization of its phosphoinositide and VP16 binding sites. *Biochemistry*, **44**, 7678–7686.
28. Houtman, J.C., Higashimoto, Y., Dimasi, N., Cho, S., Yamaguchi, H., Bowden, B., Regan, C., Malchiodi, E.L., Mariuzza, R., Schuck, P. *et al.* (2004) Binding specificity of multiprotein signaling complexes is determined by both cooperative interactions and affinity preferences. *Biochemistry*, **43**, 4170–4178.
29. Nguyen, B.D., Di Lello, P., Legault, P. and Omichinski, J.G. (2005) <sup>1</sup>H, <sup>15</sup>N, and <sup>13</sup>C resonance assignment of the amino-terminal domain of the Tfb1 subunit of yeast TFIID. *J. Biomol. NMR*, **31**, 173–174.
30. Kay, L.E., Xu, G.Y. and Yamazaki, T. (1994) Enhanced-sensitivity triple-resonance spectroscopy with minimal H<sub>2</sub>O saturation. *J. Magn. Reson. A*, **109**, 129–133.
31. Wittekind, M. and Mueller, L. (1993) HNCACB, a high-sensitivity 3D NMR experiment to correlate amide-proton and nitrogen resonances with the alpha- and beta-carbon resonances in proteins. *J. Magn. Reson. B*, **101**, 201–205.
32. Grzesiek, S. and Bax, A. (1992) Correlating backbone amide and side chain resonances in larger proteins by multiple relayed triple resonance NMR. *J. Am. Chem. Soc.*, **114**, 6291–6293.
33. Logan, T.M., Olejniczak, E.T., Xu, R.X. and Fesik, S.W. (1992) Side chain and backbone assignments in isotopically labeled proteins from two heteronuclear triple resonance experiments. *FEBS Lett.*, **314**, 413–418.
34. Ikura, M., Kay, L.E. and Bax, A. (1991) Improved three-dimensional <sup>1</sup>H-<sup>13</sup>C-<sup>1</sup>H correlation spectroscopy of a <sup>13</sup>C-labeled protein using constant-time evolution. *J. Biomol. NMR*, **1**, 299–304.
35. Yamazaki, T., Forman-Kay, J.D. and Kay, L.E. (1993) Two-dimensional NMR experiments for correlating carbon-13 beta and proton delta/epsilon chemical shifts of aromatic residues in <sup>13</sup>C-labeled proteins via scalar couplings. *J. Am. Chem. Soc.*, **115**, 11054–11055.
36. Zhang, O., Kay, L.E., Olivier, J.P. and Forman-Kay, J.D. (1994) Backbone <sup>1</sup>H and <sup>15</sup>N resonance assignments of the N-terminal SH3 domain of drk in folded and unfolded states using enhanced-sensitivity pulsed field gradient NMR techniques. *J. Biomol. NMR*, **4**, 845–858.
37. Pascal, S.M., Muhandiram, D.R., Yamazaki, T., Forman-Kay, J.D. and Kay, L.E. (1994) Simultaneous acquisition of <sup>15</sup>N- and <sup>13</sup>C-edited NOE spectra of proteins dissolved in H<sub>2</sub>O. *J. Magn. Reson.*, **103**, 197–201.
38. Delaglio, F., Grzesiek, S., Vuister, G.W., Zhu, G., Pfeifer, J. and Bax, A. (1995) NMRPipe: A multidimensional spectral processing system based on UNIX pipes. *J. Biomol. NMR*, **6**, 277–293.
39. Johnson, B.A. (2004) Using NMRView to visualize and analyze the NMR spectra of macromolecules. *Methods Mol. Biol.*, **278**, 313–352.
40. Vranken, W.F., Boucher, W., Stevens, T.J., Fogh, R.H., Pajon, A., Llinas, M., Ulrich, E.L., Markley, J.L., Ionides, J. and Laue, E.D. (2005) The CCPN data model for NMR spectroscopy: development of a software pipeline. *Proteins*, **59**, 687–696.
41. Shen, Y., Delaglio, F., Cornilescu, G. and Bax, A. (2009) TALOS+: a hybrid method for predicting protein backbone torsion angles from NMR chemical shifts. *J. Biomol. NMR*, **44**, 213–223.
42. Brunger, A.T., Adams, P.D., Clore, G.M., DeLano, W.L., Gros, P., Grosse-Kunstleve, R.W., Jiang, J.S., Kuszewski, J., Nilges, M., Pannu, N.S. *et al.* (1998) Crystallography & NMR system: a new software suite for macromolecular structure determination. *Acta Crystallogr. D Biol. Crystallogr.*, **54**, 905–921.
43. Laskowski, R.A., Rullmann, J.A., MacArthur, M.W., Kaptein, R. and Thornton, J.M. (1996) AQUA and PROCHECK-NMR: programs for checking the quality of protein structures solved by NMR. *J. Biomol. NMR*, **8**, 477–486.
44. Koradi, R., Billeter, M. and Wuthrich, K. (1996) MOLMOL: a program for display and analysis of macromolecular structures. *J. Mol. Graph.*, **14**, 51–55.
45. Tremblay, M., Teng, Y., Paquette, M., Waters, R. and Conconi, A. (2008) Complementary roles of yeast Rad4p and Rad34p in nucleotide excision repair of active and inactive rRNA gene chromatin. *Mol. Cell. Biol.*, **28**, 7504–7513.
46. den Dulk, B., Brandsma, J.A. and Brouwer, J. (2005) The Rad4 homologue YDR314C is essential for strand-specific repair of RNA polymerase I-transcribed rDNA in *Saccharomyces cerevisiae*. *Mol. Microbiol.*, **56**, 1518–1526.
47. Iben, S., Tschochner, H., Bier, M., Hoogstraten, D., Hozak, P., Egly, J.M. and Grummt, I. (2002) TFIID plays an essential role in RNA polymerase I transcription. *Cell*, **109**, 297–306.
48. den Dulk, B., Sun, S.M., de Ruijter, M., Brandsma, J.A. and Brouwer, J. (2006) Rad33, a new factor involved in nucleotide excision repair in *Saccharomyces cerevisiae*. *DNA Repair*, **5**, 683–692.
49. Stauffer, M.E. and Chazin, W.J. (2004) Structural mechanisms of DNA replication, repair, and recombination. *J. Biol. Chem.*, **279**, 30915–30918.
50. Wilson, S.H. and Kunkel, T.A. (2000) Passing the baton in base excision repair. *Nat. Struct. Biol.*, **7**, 176–178.
51. Dunand-Sauthier, I., Hohl, M., Thorel, F., Jaquier-Gubler, P., Clarkson, S.G. and Schäfer, O.D. (2005) The spacer region of XPG mediates recruitment to nucleotide excision repair complexes and determines substrate specificity. *J. Biol. Chem.*, **280**, 7030–7037.
52. Thorel, F., Constantinou, A., Dunand-Sauthier, I., Nospikel, T., Lalle, P., Raams, A., Jaspers, N.G., Vermeulen, W., Shivji, M.K., Wood, R.D. *et al.* (2004) Definition of a short region of XPG necessary for TFIID interaction and stable recruitment to sites of UV damage. *Mol. Cell. Biol.*, **24**, 10670–10680.
53. Okuda, M., Tanaka, A., Satoh, M., Mizuta, S., Takazawa, M., Ohkuma, Y. and Nishimura, Y. (2008) Structural insight into the TFIIE-TFIID interaction: TFIIE and p53 share the binding region on TFIID. *EMBO J.*, **27**, 1161–1171.
54. Di Lello, P., Miller Jenkins, L.M., Mas, C., Langlois, C., Malitskaya, E., Fradet-Turcotte, A., Archambault, J., Legault, P. and Omichinski, J.G. (2008) p53 and TFIIEalpha share a common binding site on the Tfb1/p62 subunit of TFIID. *Proc. Natl Acad. Sci. USA*, **105**, 106–111.
55. Tirode, F., Busso, D., Coin, F. and Egly, J.M. (1999) Reconstitution of the transcription factor TFIID: assignment of functions for the three enzymatic subunits, XPB, XPD and cdk7. *Mol. Cell*, **3**, 87–95.
56. Lu, H., Zawel, L., Fisher, L., Egly, J.M. and Reinberg, D. (1992) Human general transcription factor IID phosphorylates the C-terminal domain of RNA polymerase II. *Nature*, **358**, 641–645.
57. Elagoz, A., Callejo, M., Armstrong, J. and Rokeach, L.A. (1999) Although calnexin is essential in *S. pombe*, its highly conserved central domain is dispensable for viability. *J. Cell Sci.*, **112**, 4449–4460.